Atmos. Chem. Phys., 22, 11543–11555, 2022
https://doi.org/10.5194/acp-22-11543-2022

Atmospheric Chemistry and Physics
Open Access
EGU

Atmospheric oxidation mechanism and kinetics of indole initiated by ·OH and ·Cl: a computational study

Jingwen Xue[1], Fangfang Ma[1], Jonas Elm[2], Jingwen Chen[1], and Hong-Bin Xie[1]

[1]Key Laboratory of Industrial Ecology and Environmental Engineering (Ministry of Education), School of Environmental Science and Technology, Dalian University of Technology, Dalian 116024, China
[2]Department of Chemistry and iClimate, Aarhus University, Langelandsgade 140, 8000 Aarhus C, Denmark

Correspondence: Fangfang Ma (maff@dlut.edu.cn) and Hong-Bin Xie (hbxie@dlut.edu.cn)

Received: 4 February 2022 – Discussion started: 26 April 2022
Revised: 4 July 2022 – Accepted: 29 July 2022 – Published: 7 September 2022

Abstract. The atmospheric chemistry of organic nitrogen compounds (ONCs) is of great importance for understanding the formation of carcinogenic nitrosamines, and ONC oxidation products might influence atmospheric aerosol particle formation and growth. Indole is a polyfunctional heterocyclic secondary amine with a global emission quantity almost equivalent to that of trimethylamine, the amine with the highest atmospheric emission. However, the atmospheric chemistry of indole remains unclear. Herein, the reactions of indole with •OH and •Cl, and subsequent reactions of resulting indole radicals with O_2 under 200 ppt NO and 50 ppt HO_2• conditions, were investigated by a combination of quantum chemical calculations and kinetics modeling. The results indicate that •OH addition is the dominant pathway for the reaction of •OH with indole. However, both •Cl addition and H abstraction are feasible for the corresponding reaction with •Cl. All favorably formed indole radicals further react with O_2 to produce peroxy radicals, which mainly react with NO and HO_2• to form organonitrates, alkoxy radicals and hydroperoxide products. Therefore, the oxidation mechanism of indole is distinct from that of previously reported amines, which primarily form highly oxidized multifunctional compounds, imines or carcinogenic nitrosamines. In addition, the peroxy radicals from the •OH reaction can form N-(2-formylphenyl)formamide ($C_8H_7NO_2$), for the first time providing evidence for the chemical identity of the $C_8H_7NO_2$ mass peak observed in the •OH + indole experiments. More importantly, this study is the first to demonstrate that despite forming radicals by abstracting an H atom at the N site, carcinogenic nitrosamines were not produced in the indole oxidation reaction.

1 Introduction

Volatile organic compounds (VOCs) play a central role in air quality and climate change as their transformations are highly relevant for the formation of secondary organic aerosols (SOA), toxic air pollutants and ozone (O_3) (Ehn et al., 2014; Karl et al., 2018; Lewis Alastair, 2018; Li et al., 2019; Khare and Gentner, 2018; Ji et al., 2018). Therefore, an accurate description of the atmospheric transformation mechanism and kinetics of VOCs is essential to fully explore the global impacts of VOCs. Despite massive effort to understand the atmospheric fate of VOCs, current mechanism-based atmospheric models often underestimate SOA and O_3 formation quantity. Therefore, the emission inventories or reaction mechanism employed in the models are either missing some vital primary VOCs or there remain an unrevealed reaction mechanism of currently known VOCs. Hence, it is crucial to identify unaccounted reaction pathways of known VOCs or the transformation mechanism of unconsidered VOCs with high concentrations.

Organic nitrogen compounds (ONCs) are a subgroup of VOCs that are widely observed in the atmosphere (Silva et al., 2008). Until now, about 160 ONCs have been detected in the atmosphere, accounting for 10 % of total gas phase nitrogen (excluding N_2) (Ge et al., 2011; Silva et al., 2008). Due to the adverse effects of ONCs on air quality (formation of particles via acid–base reactions or generation of toxic ni-

trosamines, nitramines, isocyanic acid and low volatile products via gas phase oxidation), the chemistry of ONCs has gained significant attention in recent years (Almeida et al., 2013; Chen et al., 2017; Lin et al., 2019; Nielsen et al., 2012; Zhang et al., 2015; Xie et al., 2014, 2015, 2017; F. F. Ma et al., 2018a, 2021b, 2019; Shen et al., 2019, 2020). Detailed transformation pathways of a series of ONCs, including low-molecular-weight alkyl amines (Nicovich et al., 2015; Xie et al., 2014, 2015; F. F. Ma et al., 2021b), aromatic aniline (Xie et al., 2017; Shiels et al., 2021), heterocyclic amines (Sen-Gupta et al., 2010; Ma et al., 2018a; Borduas et al., 2016b; Ren and Da Silva, 2019) and amides (Xie et al., 2017; Borduas et al., 2016a, 2015; Bunkan et al., 2016, 2015), have been investigated. These studies have shown that the functional groups connected to the NH_x ($x = 0, 1, 2$) group highly affect the reactivity of ONCs and eventually lead to their different atmospheric impacts. Therefore, the comprehensive understanding the reaction mechanism of ONCs with various functional groups linked to the NH_x group is of great significance in assessing the atmospheric impact of ONCs.

Indole is a polyfunctional heterocyclic secondary amine (Laskin et al., 2009). Atmospheric indole has various natural and anthropogenic sources including vegetation, biomass burning, animal husbandry, coal mining, petroleum processing and the tobacco industry (Q. Ma et al., 2021; Cardoza et al., 2003; Yuan et al., 2017; Zito et al., 2015). The global emission of indole is around $0.1\,\mathrm{Tg\,yr^{-1}}$ (Misztal et al., 2015), which is almost equivalent to that of trimethylamine ($\sim 0.17\,\mathrm{Tg\,yr^{-1}}$) (Schade and Crutzen, 1995; Yu and Luo, 2014) which has the highest emission among the identified atmospheric amines. A field measurement study found that the concentration of indole can reach 1–3 ppb in ambient air during a springtime flowering event (Gentner et al., 2014). From a structural point of view, the -NH- group of indole is located at 9-center-10-electron delocalized π bonds, possibly altering its reactivity compared with that of previously well-studied aliphatic amines and aniline. Therefore, considering the large atmospheric emission of indole and its unique structure compared with previously studied amines, the reaction mechanism of indole needs to be further evaluated to assess its atmospheric impacts. Furthermore, elucidating the reaction mechanism of indole will add to the fundamental understanding of the transformation mechanism of ONCs.

Hydroxyl radicals (•OH) are considered to be the most important atmospheric oxidants governing the fate of most organic compounds (MacLeod et al., 2007). Previous experimental studies have investigated the reaction kinetics and identified the products of the •OH + indole reaction. Atkinson et al. found that the rate constant (k_{OH}) of the •OH + indole reaction is $1.54 \times 10^{-10}\,\mathrm{cm^3\,molecule^{-1}\,s^{-1}}$ at 298 K, translating to a 20 min lifetime of indole (Atkinson et al., 1995). Montoya-Aguilera et al. found that isatin and isatoic anhydride are the two dominate monomeric products for •OH initiated reaction of indole. More importantly, they found that the majority of indole oxidation products can contribute to SOA formation with an effective SOA yield of 1.3 ± 0.3 under the indole concentration (200 ppb) employed in their chamber study (Montoya-Aguilera et al., 2017). Although the chemical formulas of some of the indole oxidation products have been detected, detailed mechanistic information, such as the products branching ratio of the •OH initiated reaction of indole, remains unknown. Additionally, the lack of commercially available standards of some products presents a significant obstacle to identify the exact chemical identity of the products. Therefore, to fully understand the role of indole in SOA formation, it is essential to investigate the detailed atmospheric transformation of indole initiated by •OH.

Besides reactions with •OH, reactions with chlorine radicals (•Cl) have been proposed to be an important removal pathway for ONCs due to the identification of new •Cl continental sources and the high reactivity of •Cl (Wang et al., 2022; Li et al., 2021; Jahn et al., 2021; Xia et al., 2020; Young et al., 2014; Faxon and Allen, 2013; Riedel et al., 2012; Atkinson et al., 1989; Ji et al., 2013; Thornton et al., 2010; Le Breton et al., 2018). •Cl initiated atmospheric oxidation of ONCs can lead to the formation of N-centered radicals, once a strong 2-center-3-electron (2c–3e) bond complex has been formed between •Cl and NH_x ($x = 1, 2$) (McKee et al., 1996; Xie et al., 2015, 2017; Ma et al., 2018a). The formed N-centered radicals can further react with NO to form carcinogenic nitrosamines, increasing the atmospheric impact of ONC emissions (Xie et al., 2014, 2015, 2017; Ma et al., 2018a, 2021b; Onel et al., 2014a, b; Nielsen et al., 2012; Da Silva, 2013). As a secondary amine, indole reaction with •Cl has the possibility of forming N-centered radicals and subsequently forming nitrosamines via the reaction with NO. Since the -NH- group of indole is embedded in a unique chemical environment compared with previously well-studied ONCs, the reaction mechanism of •Cl with indole remains elusive. In addition, there are only a few studies concerning the reactions of polyfunctional heterocyclic ONCs with •Cl.

In this work, we investigated the reaction mechanism and kinetics of indole initiated by •OH and •Cl by employing a combination of quantum chemical calculations and kinetic modeling. The initial reactions of •OH and •Cl with indole and the subsequent reactions with O_2 of resulting intermediates were further investigated.

2 Computational details

2.1 Ab Initio electronic structure calculations

All the geometry optimizations and harmonic vibrational frequency calculations were performed at the M06-2X/6-31+G(d,p) level of theory (Zhao and Truhlar, 2008). Intrinsic reaction coordinate calculations were performed to confirm the connections of each transition state between the corresponding reactants and products. Single point energy calcu-

lations were performed at the CBS-QB3 method based on the geometries at the M06-2X/6-31+G(d,p) level of theory (Montgomery et al., 1999). The combination of the M06-2X functional and CBS-QB3 method has successfully been applied to predict radical–molecule reactions (Guo et al., 2020; F. F. Ma et al., 2021a; Wang et al., 2018; Wang and Wang, 2016; Wu et al., 2015; Wang et al., 2017; Fu et al., 2020). T_1 diagnostic (Table S2 in the Supplement) values in the CCSD(T) calculations within the CBS-QB3 scheme for the intermediates and transition states involved in the key reaction pathways were checked for multireference character. The T_1 diagnostic values for all checked important species in this work are lower than the threshold value of 0.045, indicating the reliability of applied single reference methods (Rienstra-Kiracofe et al., 2000). In addition, similar to our previous studies, a literature value of 0.8 kcal mol^{-1} for the isolated •Cl was used to account for the effect of spin-orbit coupling in the •Cl + indole reaction (Nicovich et al., 2015; Xie et al., 2017; Ma et al., 2018a). Atomic charges of indole and pre-reactive complexes in the •Cl + indole reaction are obtained by natural bond orbital (NBO) calculations (Reed et al., 1985). All calculations were performed within the Gaussian 09 package (Frisch et al., 2009). Throughout the paper, the symbols "R, RC, PC, TS, IM and P" stand for reactants, pre-reactive complexes, post-reactive complexes, transition states, intermediates and products involved in the reactions, respectively, and their subscripts denote different species. In addition, "A//B" was used to present the computational method, where "A" is the theoretical level for single point energy calculations and "B" is that for geometry optimizations and harmonic frequency calculations.

2.2 Kinetics calculations

MultiWell-2014.1 and MESMER 5.0 software were employed to investigate the kinetics for short time and long time reaction, respectively (Barker and Ortiz, 2001; Barker, 2001; Glowacki et al., 2012). For the initial reactions of •OH and •Cl with indole, the reaction kinetics were calculated within the MultiWell-2014.1 program. For the subsequent reactions of resulting primary intermediates, MESMER 5.0 was selected for simulating the reaction kinetics, since it has good performance for long time runs, especially for simulating the variation of the different intermediates over time. Both the MultiWell and MESMER codes employ the Rice–Ramsperger–Kassel–Marcus (RRKM) theory to calculate the reaction kinetics for reactions with intrinsic energy barriers (Holbrook, 1996; Robinson, 1972). The long-range transition-state theory (LRTST) with a dispersion force potential within the MultiWell-2014.1 program (Barker and Ortiz, 2001) or the inverse Laplace transformation (ILT) method within the MESMER 5.0 program was employed to calculate the reaction rate constants for the barrierless recombination reactions (from R to RC and P to PC) (Rienstra-Kiracofe et al., 2000). Computational details for performing LRTST and ILT calculations were described in our previous studies (F. F. Ma et al., 2021a, b; Guo et al., 2020; Ding et al., 2020). The parameters used in the LRTST calculations and Lennard-Jones parameters of intermediates estimated by the empirical method proposed by Gilbert and Smith (Gilbert and Smith, 1990) are listed in Tables S3 and S4, respectively. N_2 was selected as the buffer gas, and an average transfer energy of $\Delta E_d = 200\,cm^{-1}$ was used to simulate the collision energy transfer between active intermediates and N_2. In addition, ΔE_d between 50–250 cm^{-1} were selected to study energy transfer parameters effects. For the reactions involving H abstraction or H shift, tunneling effects were taken into account in all of the reaction rate constants calculations by using a one-dimensional unsymmetrical Eckart barrier (Eckart, 1930), and are discussed in the Supplement. The kinetic calculations were primarily performed at 298 K and 1 atm, with additional ones at 0.1, 0.4 and 0.7 atm in the troposphere relevant range to explore pressure effects. Variation in the energy transfer parameters and pressure resulted in only minor changes (< 0.1 %) in the calculated rate coefficients and branching ratios of the main reaction pathways (see details in the Supplement).

3 Results and discussion

3.1 Initial reactions of indole

In principle, •OH and •Cl could add to the unsaturated C=C bonds and benzene ring or directly abstract H atoms connected to either to a C atom or the N atom of indole. Considering the planar C_s structure of indole, •OH and •Cl addition to one side of indole was only considered here. However, although numerous attempts were made, we failed to locate the TSs and addition IMs of •Cl addition to the C2, C3, C4, C7, C8 and C9 sites of indole (the numbering of the atoms is given in Fig. 1), suggesting that such additions are in fact unfeasible. Therefore, 7 H-abstraction pathways of •OH and •Cl, respectively, 8 •OH-addition pathways and 2 •Cl-addition pathways were considered for the •OH and •Cl with indole reactions. The schematic zero-point energy (ZPE) corrected potential energy surfaces of •OH and •Cl with indole reactions are presented in Fig. 1.

As can be seen in Fig. 1, each H-abstraction reaction pathway proceeds through an RC and PC, and the addition pathways through an RC for the •OH and •Cl with indole reactions. For the H-abstraction pathways, the activation energy (E_a) for the -NH- group for both reactions are at least 2.0 kcal mol^{-1} lower than the corresponding E_a values for the -CH- groups. This indicates that H abstraction from the -NH- group forming C_8H_6N radicals and H_2O or HCl is the most favorable among all the H-abstraction pathways. In addition, the activation energy for the H abstraction from the -NH- group in the •Cl + indole reaction is much lower than the corresponding •OH + indole reaction. This is consistent with previously reported reactions of other amines with •OH

and •Cl (F. F. Ma et al., 2018a, 2021b; Xie et al., 2014, 2015, 2017; Tan et al., 2021; Ren and Da Silva, 2019; Borduas et al., 2015).

For the addition reactions, the most favorable reaction site differs for the indole + •OH and indole + •Cl reactions. Among all 8 •OH addition pathways, •OH addition to the C7 site of the C=C bond via TS_{1-7} forming IM_{1-7} is the most favorable pathway. Different from the reaction with •OH, the additions of •Cl to the C5 and C6 sites to form IM_{2-5} and IM_{2-6}, respectively, are significantly more favorable. By comparing the E_a values of the addition and H-abstraction pathways for both •OH and •Cl with indole reactions, it can be concluded that •OH addition to the C7 site is the most favorable for the •OH + indole reaction. All the •OH + indole hydrogen abstraction reactions have high energy barriers. However, the additions of •Cl to the C5 and C6 sites, as well as the -NH- H abstraction, are all favorable due to their very low E_a values for the •Cl + indole reaction.

Interestingly, we found that all the pathways for the indole + •Cl reaction can proceed via a stable 2c–3e bonded RC, which is different from that of the •OH + indole reaction. Among all 2c–3e bonded RCs, only RC_{2-10} from the -NH- abstraction pathway is formed between the N atom and •Cl, while the others are formed between the C atom and •Cl. Note that RC_{2-11}, which forms from C atom and •Cl, is the most stable among all the formed RCs in the •Cl + indole reaction. To the best of our knowledge, this is the first time that such a stable 2c–3e bonded RC has been identified between the C atom and •Cl. In addition, the energy of RC_{2-10} is higher than that of the traditional 2c–3e bonded RCs formed from alkylamine and •Cl, which would result from the delocalization of lone pair electrons of the N atom. By analyzing the NBO charges of these nine RCs (Table S5), we found that significant charge transfer occurs between •Cl and indole. The charge at the Cl atom for RC_{2-5}, RC_{2-6}, RC_{2-10}, RC_{2-11}, RC_{2-12}, RC_{2-13}, RC_{2-14}, RC_{2-15} and RC_{2-16} are $-0.35e$, $-0.33e$, $-0.31e$, $-0.39e$, $-0.35e$, $-0.33e$, $-0.39e$, $-0.35e$ and $-0.33e$, respectively, indicates that all RCs are charge-transfer complexes. Similar charge-transfer complexes were also found in our previous study of the •Cl + piperazine reaction (Ma et al., 2018a).

With the master equation theory, the overall rate constants (k_{OH} and k_{Cl}) and branching ratios (Γ) for all H-abstraction and •OH/•Cl-addition pathways involved in the •OH and •Cl with indole reactions were calculated at 298 K and 1 atm. The calculated k_{OH} and k_{Cl} values of indole are 7.9×10^{-11} and 2.9×10^{-10} cm^3 $molecule^{-1}$ s^{-1}, respectively. The calculated k_{OH} value is close to the available experimental value of 1.5×10^{-10} cm^3 $molecule^{-1}$ s^{-1} (Atkinson et al., 1995), supporting the reliability of employed computational methods. Over the temperature range 230–330 K (Ma et al., 2018b), the calculated k_{OH} and k_{Cl} values have a negative correlation with temperature (Fig. S1 in the Supplement). Based on the calculated Γ values of the •OH and •Cl with indole reactions (Table 1), it can be concluded that IM_{1-7} (77 %) is the main product for •OH + indole reaction, and IM_{2-5} (31 %), IM_{2-6} (46 %) and P_{2-10} (C_8H_6N radicals + HCl) (23 %) are the main products for •Cl + indole reaction. In addition, the calculated Γ values of IM_{1-7}, IM_{2-5}, IM_{2-6} and P_{2-10} (C_8H_6N radicals + HCl) change negligibly with the variation in temperature, pressure and energy transfer parameters (see the Supplement). Therefore, we mainly considered the further transformation of IM_{1-7}, IM_{2-5}, IM_{2-6} and C_8H_6N radicals in the following part.

Table 1. Calculated branching ratios (Γ) for the •OH and •Cl with indole reactions at 298 K and 1 atm.

Pathways	Species	Γ	Species	Γ	Species	Γ
•OH + indole	IM_{1-2}	0	IM_{1-3}	0	IM_{1-4}	5 %
	IM_{1-5}	12 %	IM_{1-6}	3 %	IM_{1-7}	77 %
	IM_{1-8}	1 %	IM_{1-9}	1 %	P_{1-10}	1 %
	P_{1-11}	0	P_{1-12}	0	P_{1-13}	0
	P_{1-14}	0	P_{1-15}	0	P_{1-16}	0
•Cl + indole	IM_{2-5}	31 %	IM_{2-6}	46 %	P_{2-10}	23 %
	P_{2-11}	0	P_{2-12}	0	P_{2-13}	0
	P_{2-14}	0	P_{2-15}	0	P_{2-16}	0

3.2 Subsequent reactions of addition intermediates

Similar to other C-centered radicals (Zhang et al., 2012; Guo et al., 2020; F. F. Ma et al., 2021a; Yu et al., 2016, 2017; Ji et al., 2017; Ding et al., 2020a), the intermediates IM_{1-7}, IM_{2-5} and IM_{2-6} will subsequently react with O_2. Two different pathways (Fig. 2) were considered for the reactions of the intermediates IM_{1-7}, IM_{2-5} and IM_{2-6} with O_2. One pathway is the direct hydrogen abstraction by O_2 from the C site connecting to the -OH or -Cl group forming P_{1-7-1} ($C_8H_7NO + HO_2$•), P_{2-5-1} ($C_8H_6NCl + HO_2$•) and P_{2-6-1} ($C_8H_6NCl + HO_2$•); the other is the O_2 addition to the C sites with high spin density (see spin density distribution in Table S10) of the intermediates IM_{1-7}, IM_{2-5} and IM_{2-6} to form peroxy radicals *Q*-*i*OO-a/s, where *Q* stands for intermediates IM_{1-7}, IM_{2-5} and IM_{2-6}, and *i* stands for the numbering of the C positions where O_2 is added. The O_2 molecule can be added to the same (-syn, abbreviated as -s) and opposite (-anti, abbreviated as -a) sides of the plane relative to the -OH or -Cl group. The C2, C4, C6 and C8 sites of IM_{1-7}, C2, C4, C6 and C8 sites of IM_{2-5} and C3, C5, C7 and C9 sites of IM_{2-6} are high spin density sites susceptible to O_2 addition.

As can be seen from the energetic data shown in Fig. 2, O_2 addition to the C4 site of IM_{1-7} to form IM_{1-7}-4OO-a/s ($-0.6/-0.6$ kcal mol^{-1}), C6 site of IM_{2-5} to form IM_{2-5}-6OO-a/s ($-0.3/-2.0$ kcal mol^{-1}) and C5 site of IM_{2-6} to form IM_{2-6}-5OO-a/s ($2.0/1.7$ kcal mol^{-1}) are the most favorable among all possible entrance pathways for the respective reactions. It deserves mentioning that the formation energy (ΔE) of IM_{2-5}-6OO-a/s and IM_{2-6}-5OO-a/s are only about 9.0 kcal mol^{-1}, which could indicate that they likely

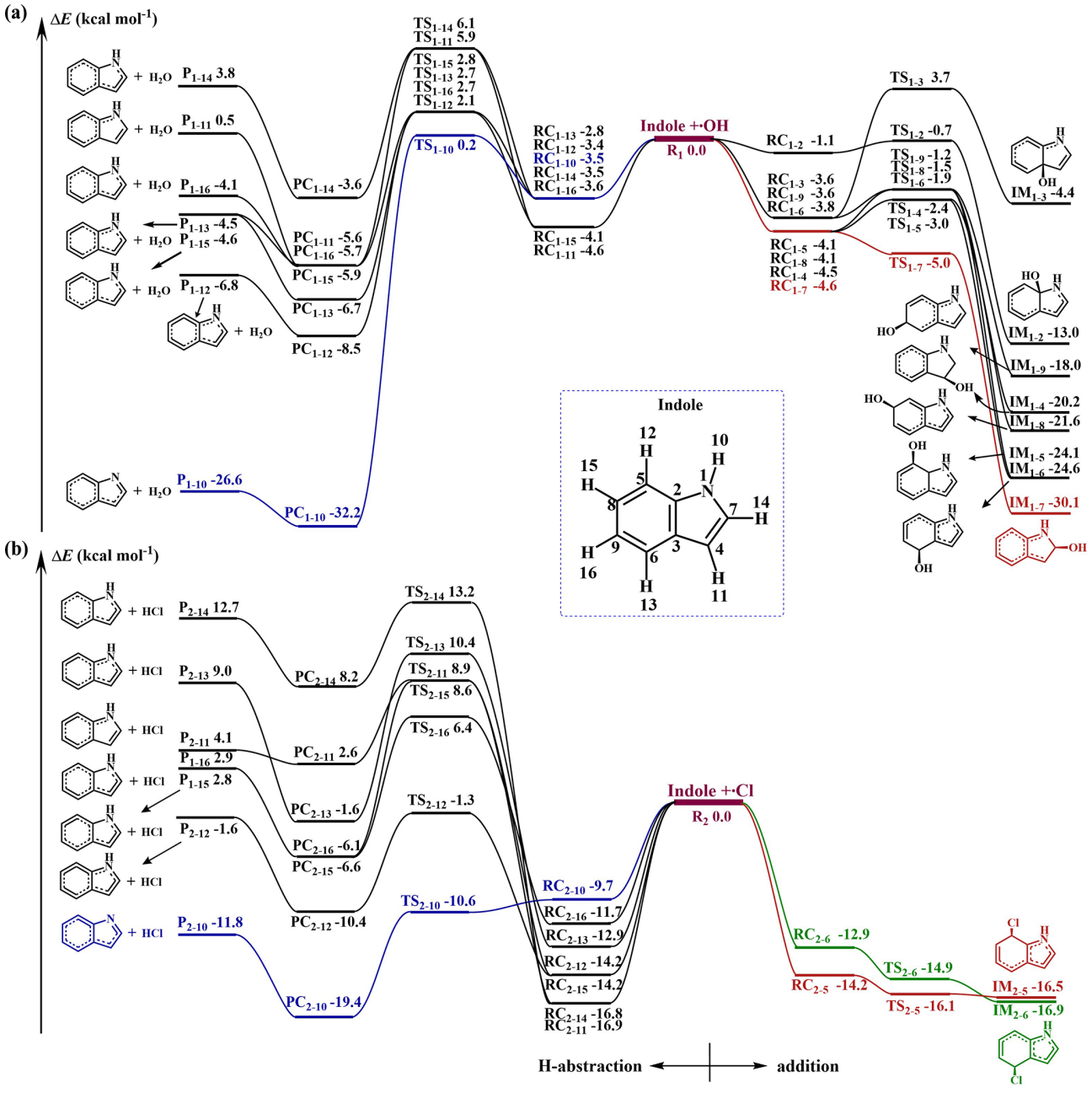

Figure 1. Schematic ZPE-corrected potential energy surface for the reactions of indole + •OH **(a)** and indole + •Cl **(b)** at the CBS-QB3//M062X/6-31+g(d,p) level of theory. The total energy of the reactants indole + •OH and indole + •Cl are set to zero, respectively (reference state).

re-dissociate back to the reactants IM_{2-5}/IM_{2-6} and O_2, if IM_{2-5}-6OO-a/s and IM_{2-6}-5OO-a/s does not rapidly transform to other species.

For the further transformation of the formed peroxy radicals IM_{1-7}-4OO(-a/s), IM_{2-5}-6OO(-a/s) and IM_{2-6}-5OO(-a/s), two transformation pathways were identified. The first pathway is cyclization reactions where the terminal O atom of -OO attacks the different C positions to form bicycle radicals *Q*-*ij*OO(-a/s) (*j* stands for the number of the C positions attacked by terminal O atom). The second pathway is H shifts from -OH, -NH- and different -CH- sites to the terminal O atom to form various hydroperoxide radicals *Q*−*i*OO-OH(-a/s), *Q*-*i*OO-NH(-a/s) and *Q*-*i*OO-C*k*H(-a/s) (*k* stands for the number of the C positions from which H is shifted), respectively. For IM_{1-7}-4OO(-a/s) and IM_{2-5}-6OO(-a/s), forming IM_{1-7}-4OO-OH-s and IM_{2-5}-6OO-C5H-a via H-shift reactions are the most favorable, respectively. However, for IM_{2-6}-5OO(-a/s), the cyclization

reaction forming IM_{2-6}-52OO-a is the most favorable. It is noted that the formed IM_{1-7}-4OO-OH-s from IM_{1-7}-4OO(-a/s) can barrierlessly transform to form $C_8H_7NO_2$ (N-(2-formylphenyl)formamide) and •OH (collectively denoted $P_{1-7-4-1}$) via concerted C-C and O-O bonds rupture. The further transformation of the peroxy radicals IM_{1-7}-4OO(-a/s), IM_{2-5}-6OO(-a/s) and IM_{2-6}-5OO(-a/s) needs to overcome barriers above 20.5 kcal mol^{-1} (relative to their respective peroxy radicals), indicating that the further transformation of IM_{1-7}-4OO(-a/s), IM_{2-5}-6OO(-a/s) and IM_{2-6}-5OO(-a/s) should be very slow.

Based on the energetic data of the favorable reaction pathways, MESMER modeling was employed to investigate the reaction rate constants and fractional yields for the reactions of IM_{1-7}, IM_{2-5} and IM_{2-6} with O_2. Similar to previous studies (Guo et al., 2020; F. F. Ma et al., 2021a, b; Zhang et al., 2012; Fu et al., 2020; Crounse et al., 2013; Veres et al., 2020), bimolecular reactions with NO and HO_2• are considered as competitive pathways for the unimolecular reactions of the peroxy radicals IM_{1-7}-4OO(-a/s), IM_{2-5}-6OO(-a/s) and IM_{2-6}-5OO(-a/s) by simply adding their pseudo-first-order rate constants into the master equation modeling. Here, applied pseudo-first-order rate constants for peroxy radicals (IM_{1-7}-4OO(-a/s), IM_{2-5}-6OO(-a/s) and IM_{2-6}-5OO(-a/s)) reaction with NO and HO_2• are 0.06 and 0.02 s^{-1}, respectively, corresponding to reactions occurring at 200 ppt NO and 50 ppt HO_2• conditions (Hofzumahaus et al., 2009; Yu et al., 2020; Praske et al., 2018). The reactions of peroxy radicals with NO and HO_2• should form organonitrate/alkoxy radicals (collectively denoted NO-P_n, where n marks products from the different peroxy radical reactions) and hydroperoxide (HO_2-P_n), respectively. Pseudo-first-order rate constants of IM_{1-7}, IM_{2-5}, and IM_{2-6} with O_2 are calculated to be 3.0×10^7 s^{-1}, based on the reaction rate constants of IM_{1-7}, IM_{2-5}, and IM_{2-6} with O_2 (6.0×10^{-12} cm^3 $molecule^{-1}$ s^{-1}) and the concentration of O_2 ($[O_2] = 5.0 \times 10^{18}$ molecule cm^{-1}). The simulated time-dependent fractional yields are presented in Fig. 3.

As can be seen in Fig. 3, after 100 s, the reactions of IM_{1-7}, IM_{2-5} and IM_{2-6} with O_2 mainly form the organonitrate/alkoxy radicals NO-P_3 ($C_8H_8N_2O_3$/$C_8H_8NO_2$•), NO-P_4 ($C_8H_7N_2O_3Cl$/C_8H_7NClO•) and NO-P_5 ($C_8H_7N_2O_3Cl$/C_8H_7NClO•), followed by the formation of hydroperoxide HO_2-P_3 ($C_8H_9NO_3$), HO_2-P_4 ($C_8H_8NO_2Cl$) and HO_2-P_5 ($C_8H_8NO_2Cl$), respectively. For the reactions of IM_{2-5} and IM_{2-6} with O_2, the main products formed are NO-$P_{4/5}$ and HO_2-$P_{4/5}$. In contrast, the $IM_{1-7} + O_2$ reaction also leads to the fragmental products $P_{1-7-4-1}$ ($C_8H_7NO_2$ and •OH) besides the main products NO-P_3 and HO_2-P_3. This difference in product branching ratios is due to the fact that the peroxy radical IM_{1-7}-4OO(-a/s) has a lower unimolecular reaction energy barrier than IM_{2-5}-6OO(-a/s) and IM_{2-6}-5OO(-a/s). It should be noted that the $C_8H_7NO_2$ product has been detected in previous experimental study of

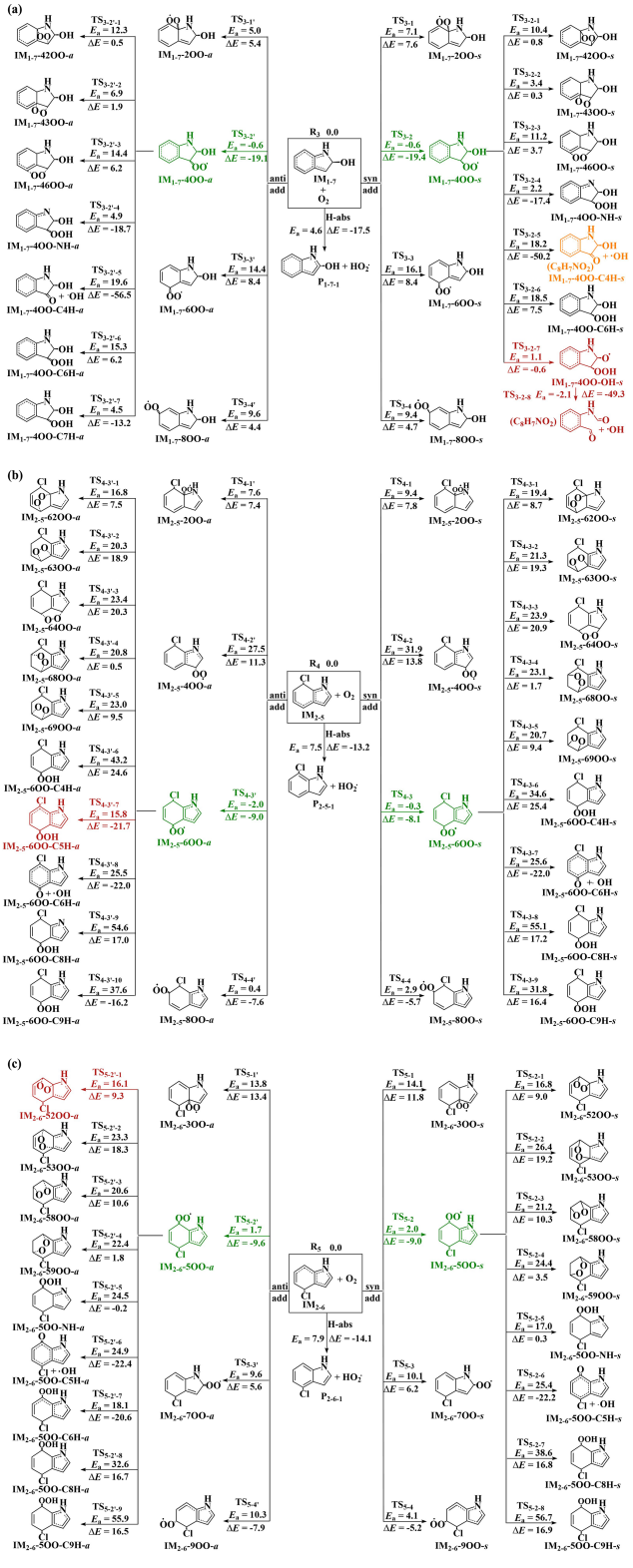

Figure 2. Reaction pathways and corresponding energetic data for the reactions of IM_{1-7} **(a)**, IM_{2-5} **(b)** and IM_{2-6} **(c)** with O_2. Units are in kcal mol^{-1}.

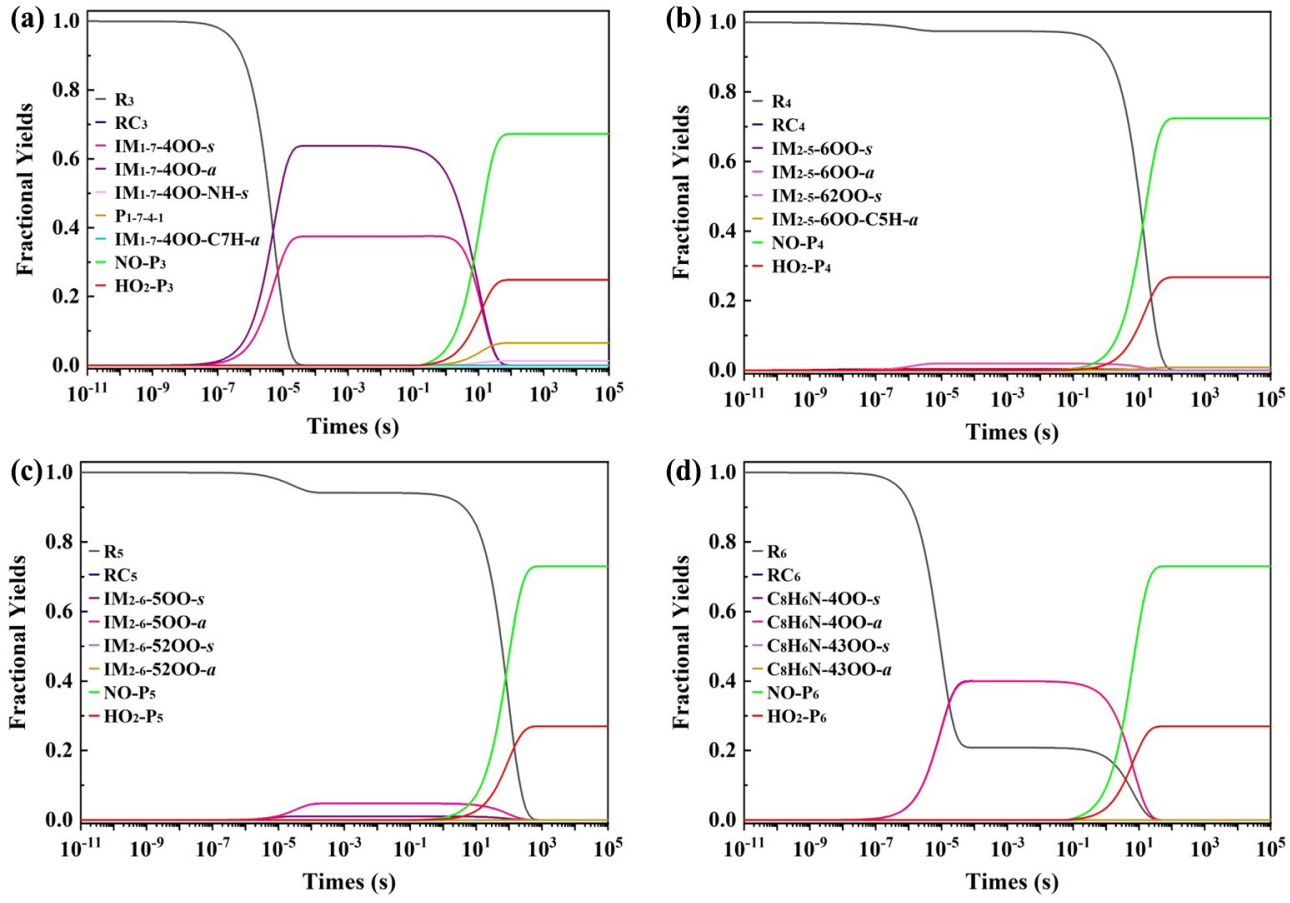

Figure 3. Calculated fractional yields of species (at 200 ppt NO and 50 ppt HO_2• conditions) as a function of time in the reactions of IM_{1-7} **(a)**, IM_{2-5} **(b)**, IM_{2-6} **(c)** and C_8H_6N **(d)** with O_2 at 298 K and 1 atm.

the •OH + indole reaction (Montoya-Aguilera et al., 2017), supporting the validity of our computational results.

An obvious difference for these three reactions is that the reaction of IM_{1-7} with O_2 can form peroxy radicals IM_{1-7}-4OO(-a/s) with high yields during the reactions. However, the yields of the corresponding peroxy radicals IM_{2-5}-6OO(-a/s) and IM_{2-6}-5OO(-a/s) from the reactions of IM_{2-5} and IM_{2-6} with O_2 are low. The difference mainly originates from the difference in the formation energy of these three peroxy radicals as shown in Fig. 2. The ΔE values of IM_{1-7}-4OO(-a/s) ($-19.1/-19.4$ kcal mol^{-1}) are much lower than those of IM_{2-5}-6OO(-a/s) ($-9.0/-8.1$ kcal mol^{-1}) and IM_{2-6}-5OO(-a/s) ($-9.6/-9.0$ kcal mol^{-1}). As discussed above, the high formation energy of IM_{2-5}-6OO(-a/s) and IM_{2-6}-5OO(-a/s) should make IM_{2-5}-6OO(-a/s) and IM_{2-6}-5OO(-a/s) return back to the reactants, explaining the reason for the lower yields of IM_{2-5}-6OO(-a/s) and IM_{2-6}-5OO(-a/s).

3.3 Subsequent reactions of C_8H_6N radicals from the H-abstraction pathway

Here, the bimolecular reaction with O_2 was mainly considered for C_8H_6N radicals as its sole atmospheric fate. It was found that the spin density distribution was mainly centered at the C atoms (C4 (0.662), C6 (0.261), C8 (0.178)) and N atom (0.256), indicating that the C_8H_6N radical is delocalized. This is in contrast to previously studied N-centered radicals formed from alkylamine oxidation, which is highly localized (Xie et al., 2015, 2014; Ma et al., 2018a; Tan et al., 2021; Borduas et al., 2015). Therefore, O_2 addition to the C4, C6, C8 and N1 sites (including attack from both sides) is considered for the reaction of the C_8H_6N radicals with O_2. As can be seen in Fig. 4, O_2 additions to the C4 site of the C_8H_6N radicals forming C_8H_6N-4OO-a/s with E_a of -0.3 kcal mol^{-1} are the most favorable, translating to pseudo-first-order reaction rate constants of 3.0×10^7 s^{-1}. Such rate constants are about 7 orders of magnitude higher than that of typical N-centered radicals reacting with NO even under very high NO concentration (5 ppb). Therefore, C_8H_6N radicals do not react with NO to form carcinogenic

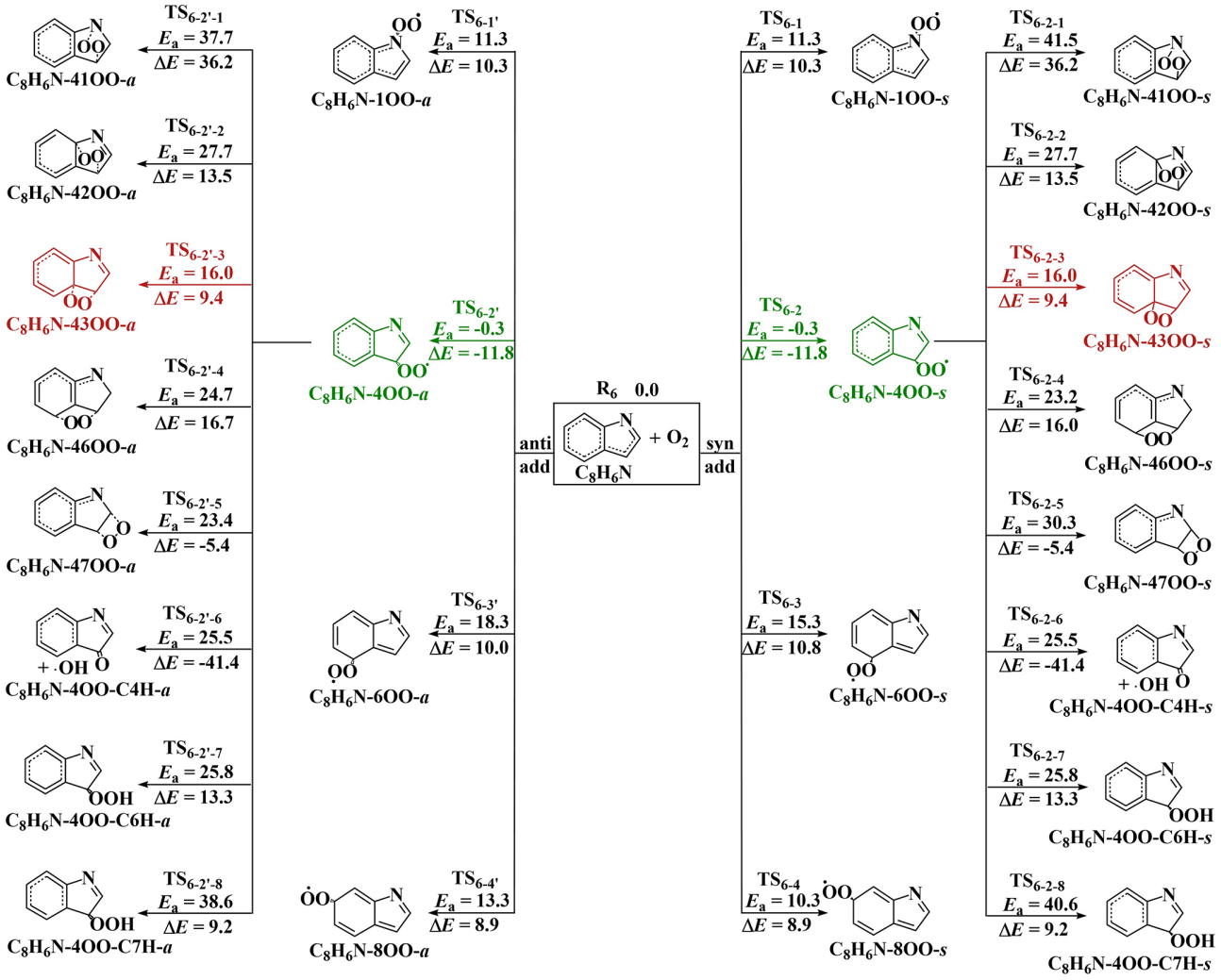

Figure 4. Reaction pathways and corresponding energetic data for the reactions of C_8H_6N radicals with O_2. Units are in kcal mol^{-1}.

nitrosamines in any appreciable amount, which is different from the previously reported reaction mechanism of N-centered radicals formed from the reactions of alkylamines with •Cl (Xie et al., 2015, 2014; Ma et al., 2018a). To the best of our knowledge, this is the first study to reveal that despite forming radicals by abstracting an H atom at the N site, carcinogenic nitrosamines were not produced in the indole oxidation reaction.

For the transformation of the formed C_8H_6N-4OO-a/s radicals, the ring closure reaction to form C_8H_6N-43OO-a/s is the most favorable, but it still needs to overcome a 27.8 kcal mol^{-1} energy barrier; therefore, the further transformation of the formed C_8H_6N-4OO-a/s should proceed very slowly. The C_8H_6N-4OO-a/s should mainly react with NO and HO_2• to form NO-P_6 and HO_2-P_6. Detailed kinetics calculations (Fig. 3d) further confirm that the reaction of C_8H_6N radicals with O_2 mainly form NO-P_6 and HO_2-P_6 under 200 ppt NO and 50 ppt HO_2• conditions.

4 Comparison with available experimental results and atmospheric implications

This study found that •OH and •Cl initiated reactions of indole mainly form organonitrates, alkoxy radicals and hydroperoxide products with N-(2-formylphenyl)formamide ($C_8H_7NO_2$) as a minor product at 200 ppt NO and 50 ppt HO_2• conditions. The formed closed-shell products have high oxygen-to-carbon ratios compared with indole and therefore are expected to have lower vapor pressures, likely being first generation products that can be further oxidized and contribute to the formation of SOA.

With our findings, a comparison was made with the available experimental study on •OH initiated reaction of indole. The calculated k_{OH} value (7.9×10^{-11} cm^3 molecule^{-1} s^{-1}) of indole is consistent with the experimental value (15×10^{-11} cm^3 molecule^{-1} s^{-1}) (Atkinson et al., 1995), indicating the reliability of applied theoretical methods. A signal with the molecular formula $C_8H_7NO_2$ has been ob-

served in the mass spectrum in an experimental study by Montoya-Aguilera et al. (2017), supporting the formation of the predicted N-(2-formylphenyl)formamide. To the best of our knowledge, our study is the first to reveal the chemical identity of the mass spectrum signal as N-(2-formylphenyl)formamide, as opposed to the proposed 3-oxy-2-hydroxy-indole. In addition, monomeric products (isatin and isatoic anhydride) and dimer products have not been observed in our computational study. We speculate that they may be produced from the subsequent conversion of the formed alkoxy radicals, multi-generation reactions of organonitrates and hydroperoxide as well as self- or cross reactions of peroxy radicals ($RO_2 + RO_2$). Therefore, further studies are warranted to investigate the subsequent transformation of the formed alkoxy radicals, organonitrates and hydroperoxide, and the $RO_2 + RO_2$ reactions, to accurately describe the atmospheric impact of indole.

The calculated k_{Cl} value of the indole + •Cl reaction is a factor of 3.7 higher than that of the indole + •OH reaction, and is close to the k_{Cl} values for the reactions of alkylamines, heterocyclic amines and amides with •Cl (Xie et al., 2017, 2015; Ma et al., 2018a; Nicovich et al., 2015). The contribution of •Cl to the transformation of indole is calculated to be 3.6 %–36 % that of •OH, assuming •Cl concentrations equal to 1 %–10 % of that of •OH (Wang and Ruiz, 2017; Nicovich et al., 2015; Xie et al., 2017, 2015; Ma et al., 2018a). Therefore, •Cl plays an important role in the overall transformation of indole. More importantly, •Cl initiated reaction of indole does not lead to the formation of carcinogenic nitrosamines although •Cl can favorably abstract the H atom from the N site to form C_8H_6N radicals, which is a plausible precursor of carcinogenic nitrosamines. Hence, to the best of our knowledge, this is the first study to reveal that despite forming radicals by abstracting an H atom at the N site, carcinogenic nitrosamines were not produced in the indole oxidation reaction. This is most likely caused by the delocalized character of the formed C_8H_6N radicals due to the existence of the adjacent unsaturated bonds. Therefore, this study further confirms that the functional groups connected to the NH_x ($x = 1, 2$) group highly affect the atmospheric fate of ONCs. Further studies should be performed to investigate the structure–activity relationship of •Cl initiated reactions of ONCs to comprehensively evaluate their atmospheric impacts.

Data availability. The data in this article are available from the corresponding author upon request (maff@dlut.edu.cn, hbxie@dlut.edu.cn).

Supplement. The supplement related to this article is available online at: https://doi.org/10.5194/acp-22-11543-2022-supplement.

Author contributions. FM and HBX designed the research model; JX, FM and HBX performed the research; JX, FM and HBX analyzed the data; JX, FM, JE, HBX and JC wrote the paper; and FM, HBX, JE and JC reviewed and revised the paper.

Competing interests. The contact author has declared that none of the authors has any competing interests.

Disclaimer. Publisher's note: Copernicus Publications remains neutral with regard to jurisdictional claims in published maps and institutional affiliations.

Acknowledgements. We thank Struan H. Robertson (Dassault Systèmes) for the discussion on the MESMER simulations. The study was supported by National Natural Science Foundation of China (grant nos. 22176022, 21876024), the LiaoNing Revitalization Talents Program (grant no. XLYC1907194), the Major International (Regional) Joint Research Project (grant no. 21661142001) and the Supercomputing Center of Dalian University of Technology.

Financial support. This research has been supported by the National Natural Science Foundation of China (grant nos. 22176022, 21876024), the LiaoNing Revitalization Talents Program (grant no. XLYC1907194) and the Major International (Regional) Joint Research Project (grant no. 21661142001).

Review statement. This paper was edited by John Liggio and reviewed by two anonymous referees.

References

Almeida, J., Schobesberger, S., Kürten, A., Ortega, I. K., Kupiainen-Määttä, O., Praplan, A. P., Adamov, A., Amorim, A., Bianchi, F., Breitenlechner, M., David, A., Dommen, J., Donahue, N. M., Downard, A., Dunne, E., Duplissy, J., Ehrhart, S., Flagan, R. C., Franchin, A., Guida, R., Hakala, J., Hansel, A., Heinritzi, M., Henschel, H., Jokinen, T., Junninen, H., Kajos, M., Kangasluoma, J., Keskinen, H., Kupc, A., Kurtén, T., Kvashin, A. N., Laaksonen, A., Lehtipalo, K., Leiminger, M., Leppä, J., Loukonen, V., Makhmutov, V., Mathot, S., McGrath, M. J., Nieminen, T., Olenius, T., Onnela, A., Petäjä, T., Riccobono, F., Riipinen, I., Rissanen, M., Rondo, L., Ruuskanen, T., Santos, F. D., Sarnela, N., Schallhart, S., Schnitzhofer, R., Seinfeld, J. H., Simon, M., Sipilä, M., Stozhkov, Y., Stratmann, F., Tomé, A., Tröstl, J., Tsagkogeorgas, G., Vaattovaara, P., Viisanen, Y., Virtanen, A., Vrtala, A., Wagner, P. E., Weingartner, E., Wex, H., Williamson, C., Wimmer, D., Ye, P., Yli-Juuti, T., Carslaw, K. S., Kulmala, M., Curtius, J., Baltensperger, U., Worsnop, D. R., Vehkamäki, H., and Kirkby, J.: Molecular understanding of sulphuric acid-amine particle nucleation in the atmosphere, Nature, 502, 359–363, https://doi.org/10.1038/nature12663, 2013.

Atkinson, R., Baulch, D. L., Cox, R. A., Hampson, R. F., Kerr, J. A., and Troe, J.: Evaluated Kinetic and Photochemical Data for Atmospheric Chemistry: Supplement III. IUPAC Subcommittee on Gas Kinetic Data Evaluation for Atmospheric Chemistry, J. Phys. Chem. Ref. Data, 18, 881–1097, https://doi.org/10.1063/1.555832, 1989.

Atkinson, R., Tuazon, E. C., Arey, J., and Aschmann, S. M.: Atmospheric and indoor chemistry of gas-phase indole, quinoline, and isoquinoline, Atmos. Environ., 29, 3423–3432, https://doi.org/10.1016/1352-2310(95)00103-6, 1995.

Barker, J. R.: Multiple-well, multiple-path unimolecular reaction systems. I. MultiWell computer program suite, Int. J. Chem. Kinet., 33, 232–245, https://doi.org/10.1002/kin.1017, 2001.

Barker, J. R. and Ortiz, N. F.: Multiple-Well, multiple-path unimolecular reaction systems. II. 2-methylhexyl free radicals, Int. J. Chem. Kinet., 33, 246–261, https://doi.org/10.1002/kin.1018, 2001.

Borduas, N., da Silva, G., Murphy, J. G., and Abbatt, J. P. D.: Experimental and Theoretical Understanding of the Gas Phase Oxidation of Atmospheric Amides with OH Radicals: Kinetics, Products, and Mechanisms, J. Phys. Chem. A, 119, 4298–4308, https://doi.org/10.1021/jp503759f, 2015.

Borduas, N., Abbatt, J. P. D., Murphy, J. G., So, S., and da Silva, G.: Gas-Phase Mechanisms of the Reactions of Reduced Organic Nitrogen Compounds with OH Radicals, Environ. Sci. Technol., 50, 11723–11734, https://doi.org/10.1021/acs.est.6b03797, 2016a.

Borduas, N., Murphy, J. G., Wang, C., da Silva, G., and Abbatt, J. P. D.: Gas Phase Oxidation of Nicotine by OH Radicals: Kinetics, Mechanisms, and Formation of HNCO, Environ. Sci. Technol. Lett., 3, 327–331, https://doi.org/10.1021/acs.estlett.6b00231, 2016b.

Bunkan, A. J. C., Hetzler, J., Mikoviny, T., Wisthaler, A., Nielsen, C. J., and Olzmann, M.: The reactions of N-methylformamide and N,N-dimethylformamide with OH and their photo-oxidation under atmospheric conditions: experimental and theoretical studies, Phys. Chem. Chem. Phys., 17, 7046–7059, https://doi.org/10.1039/C4CP05805D, 2015.

Bunkan, A. J. C., Mikoviny, T., Nielsen, C. J., Wisthaler, A., and Zhu, L.: Experimental and Theoretical Study of the OH-Initiated Photo-oxidation of Formamide, J. Phys. Chem. A, 120, 1222–1230, https://doi.org/10.1021/acs.jpca.6b00032, 2016.

Cardoza, Y. J., Lait, C. G., Schmelz, E. A., Huang, J., and Tumlinson, J. H.: Fungus-Induced Biochemical Changes in Peanut Plants and Their Effect on Development of Beet Armyworm, Spodoptera Exigua Hübner (Lepidoptera: Noctuidae) Larvae, Environ. Entomol., 32, 220–228, https://doi.org/10.1603/0046-225X-32.1.220, 2003.

Chen, J., Jiang, S., Liu, Y.-R., Huang, T., Wang, C. Y., Miao, S. K., Wang, Z. Q., Zhang, Y., and Huang, W.: Interaction of oxalic acid with dimethylamine and its atmospheric implications, RSC Adv., 7, 6374–6388, https://doi.org/10.1039/C6RA27945G, 2017.

Crounse, J. D., Nielsen, L. B., Jørgensen, S., Kjaergaard, H. G., and Wennberg, P. O.: Autoxidation of Organic Compounds in the Atmosphere, J. Phys. Chem. Lett., 4, 3513–3520, https://doi.org/10.1021/jz4019207, 2013.

da Silva, G.: Formation of Nitrosamines and Alkyldiazohydroxides in the Gas Phase: The CH_3NH + NO Reaction Revisited, Environ. Sci. Technol., 47, 7766–7772, https://doi.org/10.1021/es401591n, 2013.

Ding, Z., Yi, Y., Wang, W., and Zhang, Q.: Atmospheric oxidation of indene initiated by OH radical in the presence of O_2 and NO: A mechanistic and kinetic study, Chemosphere, 259, 127331, https://doi.org/10.1016/j.chemosphere.2020.127331, 2020a.

Ding, Z., Yi, Y., Wang, W., and Zhang, Q.: Understanding the role of Cl and NO_3 radicals in initiating atmospheric oxidation of fluorene: A mechanistic and kinetic study, Sci. Total Environ., 716, 136905, https://doi.org/10.1016/j.scitotenv.2020.136905, 2020b.

Eckart, C.: The penetration of a potential barrier by electrons, Phys. Rev., 35, 1303–1309, https://doi.org/10.1103/PhysRev.35.1303, 1930.

Ehn, M., Thornton, J. A., Kleist, E., Sipilä, M., Junninen, H., Pullinen, I., Springer, M., Rubach, F., Tillmann, R., Lee, B., Lopez-Hilfiker, F., Andres, S., Acir, I.-H., Rissanen, M., Jokinen, T., Schobesberger, S., Kangasluoma, J., Kontkanen, J., Nieminen, T., Kurtén, T., Nielsen, L. B., Jørgensen, S., Kjaergaard, H. G., Canagaratna, M., Maso, M. D., Berndt, T., Petäjä, T., Wahner, A., Kerminen, V.-M., Kulmala, M., Worsnop, D. R., Wildt, J., and Mentel, T. F.: A large source of low-volatility secondary organic aerosol, Nature, 506, 476–479, https://doi.org/10.1038/nature13032, 2014.

Faxon, C. B. and Allen, D. T.: Chlorine chemistry in urban atmospheres: a review, Environ. Chem., 10, 221–233, https://doi.org/10.1071/en13026, 2013.

Frisch, M. J., Trucks, G. W., Schlegel, H. B., Scuseria, G. E., Robb, M. A., Cheeseman, J. R., Scalmani, G., Barone, V., Mennucci, B., Petersson, G. A., Nakatsuji, H., Caricato, M., Li, X., Hratchian, H. P., Izmaylov, A. F., Bloino, J., Zheng, G., Sonnenberg, J. L., Hada, M., Ehara, M., Toyota, K., Fukuda, R., Hasegawa, J., Ishida, M., Nakajima, T., Honda, Y., Kitao, O., Nakai, H., Vreven, T., Montgomery Jr., J. A., Peralta, J. E., Ogliaro, F., Bearpark, M., Heyd, J. J., Brothers., E., Kudin, K. N., Staroverov, V. N., Kobayashi, R., Normand, J., Raghavachari, K., Rendell, A., Burant, J. C., Iyengar, S. S., Tomasi, J., Cossi, M., Rega, N., Millam, J. M., Klene, M., Knox, J. E., Cross, J. B., Bakken, V., Adamo, C., Jaramillo, J., Gomperts, R., Stratmann, R. E., Yazyev., O., Austin, A. J., Cammi, R., Pomelli, C., Ochterski, J. W., Martin., R. L., Morokuma, K., Zakrzewski, V. G., Voth, G. A., Salvador, P.; Dannenberg, J. J., Dapprich, S., Daniels, A. D., Farkas, O., Foresman, J. B., Ortiz, J. V., Cioslowski, J., and Fox, D. J.: Gaussian 09, Gaussian, Inc., Wallingford CT, 2009.

Fu, Z., Xie, H. B., Elm, J., Guo, X., Fu, Z., and Chen, J.: Formation of Low-Volatile Products and Unexpected High Formaldehyde Yield from the Atmospheric Oxidation of Methylsiloxanes, Environ. Sci. Technol., 54, 7136–7145, https://doi.org/10.1021/acs.est.0c01090, 2020.

Ge, X., Wexler, A. S., and Clegg, S. L.: Atmospheric amines – Part I. A review, Atmos. Environ., 45, 524–546, https://doi.org/10.1016/j.atmosenv.2010.10.012, 2011.

Gentner, D. R., Ormeño, E., Fares, S., Ford, T. B., Weber, R., Park, J.-H., Brioude, J., Angevine, W. M., Karlik, J. F., and Goldstein, A. H.: Emissions of terpenoids, benzenoids, and other biogenic gas-phase organic compounds from agricultural crops and their potential implications for air quality, Atmos. Chem. Phys., 14, 5393–5413, https://doi.org/10.5194/acp-14-5393-2014, 2014.

Gilbert, R. G. and Smith, S. C: Theory of Unimolecular and Recombination Reactions, Blackwell Scientific, Carlton, Australia, ISBN-10 0632027495, 1990.

Glowacki, D. R., Liang, C.-H., Morley, C., Pilling, M. J., and Robertson, S. H.: MESMER: An Open-Source Master Equation Solver for Multi-Energy Well Reactions, J. Phys. Chem. A, 116, 9545–9560, https://doi.org/10.1021/jp3051033, 2012.

Guo, X., Ma, F., Liu, C., Niu, J., He, N., Chen, J., and Xie, H. B.: Atmospheric oxidation mechanism and kinetics of isoprene initiated by chlorine radicals: A computational study, Sci. Total Environ., 712, 136330, https://doi.org/10.1016/j.scitotenv.2019.136330, 2020.

Hofzumahaus, A., Rohrer, F., Lu, K., Bohn, B., Brauers, T., Chang, C.-C., Fuchs, H., Holland, F., Kita, K., Kondo, Y., Li, X., Lou, S., Shao, M., Zeng, L., Wahner, A., and Zhang, Y.: Amplified Trace Gas Removal in the Troposphere, Science, 324, 1702–1704, https://doi.org/10.1126/science.1164566, 2009.

Holbrook, K. A, Pilling, M. J., Robertson, S. H., and Robinson, P. J.: Unimolecular Reactions, 2nd edn., Wiley, New York, ISBN 0471922684, 1996.

Jahn, L. G., Wang, D. S., Dhulipala, S. V., and Hildebrandt Ruiz, L.: Gas-phase chlorine radical oxidation of alkanes: Effects of structural branching, NO_x, and relative humidity observed during environmental chamber experiments, J. Phys. Chem. A, 125, 7303–7317, https://doi.org/10.1021/acs.jpca.1c03516, 2021.

Ji, Y., Zhao, J., Terazono, H., Misawa, K., Levitt, N. P., Li, Y., Lin, Y., Peng, J., Wang, Y., Duan, L., Pan, B., Zhang, F., Feng, X., An, T., Marrero-Ortiz, W., Secrest, J., Zhang, A. L., Shibuya, K., Molina, M. J., and Zhang, R.: Reassessing the atmospheric oxidation mechanism of toluene, P. Natl. Acad. Sci. USA, 114, 8169, https://doi.org/10.1073/pnas.1705463114, 2017.

Ji, Y., Zheng, J., Qin, D., Li, Y., Gao, Y., Yao, M., Chen, X., Li, G., An, T., and Zhang, R.: OH-Initiated Oxidation of Acetylacetone: Implications for Ozone and Secondary Organic Aerosol Formation, Environ. Sci. Technol., 52, 11169–11177, https://doi.org/10.1021/acs.est.8b03972, 2018.

Ji, Y. M., Wang, H. H., Gao, Y. P., Li, G. Y., and An, T. C.: A theoretical model on the formation mechanism and kinetics of highly toxic air pollutants from halogenated formaldehydes reacted with halogen atoms, Atmos. Chem. Phys., 13, 11277–11286, https://doi.org/10.5194/acp-13-11277-2013, 2013.

Karl, T., Striednig, M., Graus, M., Hammerle, A., and Wohlfahrt, G.: Urban flux measurements reveal a large pool of oxygenated volatile organic compound emissions, P. Natl. Acad. Sci. USA, 115, 1186, https://doi.org/10.1073/pnas.1714715115, 2018.

Khare, P. and Gentner, D. R.: Considering the future of anthropogenic gas-phase organic compound emissions and the increasing influence of non-combustion sources on urban air quality, Atmos. Chem. Phys., 18, 5391–5413, https://doi.org/10.5194/acp-18-5391-2018, 2018.

Laskin, A., Smith, J. S., and Laskin, J.: Molecular Characterization of Nitrogen-Containing Organic Compounds in Biomass Burning Aerosols Using High-Resolution Mass Spectrometry, Environ. Sci. Technol., 43, 3764–3771, https://doi.org/10.1021/es803456n, 2009.

Le Breton, M., Hallquist, Å. M., Pathak, R. K., Simpson, D., Wang, Y., Johansson, J., Zheng, J., Yang, Y., Shang, D., Wang, H., Liu, Q., Chan, C., Wang, T., Bannan, T. J., Priestley, M., Percival, C. J., Shallcross, D. E., Lu, K., Guo, S., Hu, M., and Hallquist, M.: Chlorine oxidation of VOCs at a semi-rural site in Beijing: significant chlorine liberation from $ClNO_2$ and subsequent gas- and particle-phase Cl–VOC production, Atmos. Chem. Phys., 18, 13013–13030, https://doi.org/10.5194/acp-18-13013-2018, 2018.

Lewis Alastair, C.: The changing face of urban air pollution, Science, 359, 744–745, https://doi.org/10.1126/science.aar4925, 2018.

Li, J., Zhang, N., Wang, P., Choi, M., Ying, Q., Guo, S., Lu, K., Qiu, X., Wang, S., Hu, M., Zhang, Y., and Hu, J.: Impacts of chlorine chemistry and anthropogenic emissions on secondary pollutants in the Yangtze river delta region, Environ. Pollut., 287, 117624, https://doi.org/10.1016/j.envpol.2021.117624, 2021.

Li, K., Li, J., Tong, S., Wang, W., Huang, R.-J., and Ge, M.: Characteristics of wintertime VOCs in suburban and urban Beijing: concentrations, emission ratios, and festival effects, Atmos. Chem. Phys., 19, 8021–8036, https://doi.org/10.5194/acp-19-8021-2019, 2019.

Lin, Y., Ji, Y., Li, Y., Secrest, J., Xu, W., Xu, F., Wang, Y., An, T., and Zhang, R.: Interaction between succinic acid and sulfuric acid–base clusters, Atmos. Chem. Phys., 19, 8003–8019, https://doi.org/10.5194/acp-19-8003-2019, 2019.

Ma, F. F., Ding, Z. Z., Elm, J., Xie, H. B., Yu, Q., Liu, C., Li, C., Fu, Z., Zhang, L., and Chen, J.: Atmospheric Oxidation of Piperazine Initiated by •Cl: Unexpected High Nitrosamine Yield, Environ. Sci. Technol., 52, 9801–9809, https://doi.org/10.1021/acs.est.8b02510, 2018a.

Ma, F. F., Xie, H. B., and Chen, J.: Benchmarking of DFT functionals for the kinetics and mechanisms of atmospheric addition reactions of OH radicals with phenyl and substituted phenyl-based organic pollutants, Int. J. Quantum Chem., 118, e25533, https://doi.org/10.1002/qua.25533, 2018b.

Ma, F. F., Xie, H. B., Elm, J., Shen, J., Chen, J., and Vehkamäki, H.: Piperazine Enhancing Sulfuric Acid-Based New Particle Formation: Implications for the Atmospheric Fate of Piperazine, Environ. Sci. Technol., 53, 8785–8795, https://doi.org/10.1021/acs.est.9b02117, 2019.

Ma, F. F., Guo, X. R., Xia, D. M., Xie, H. B., Wang, Y., Elm, J., Chen, J., and Niu, J.: Atmospheric Chemistry of Allylic Radicals from Isoprene: A Successive Cyclization-Driven Autoxidation Mechanism, Environ. Sci. Technol., 55, 4399–4409, https://doi.org/10.1021/acs.est.0c07925, 2021a.

Ma, F. F., Xie, H.-B., Li, M., Wang, S., Zhang, R., and Chen, J.: Autoxidation mechanism for atmospheric oxidation of tertiary amines: Implications for secondary organic aerosol formation, Chemosphere, 273, 129207, https://doi.org/10.1016/j.chemosphere.2020.129207, 2021b.

Ma, Q., Meng, N., Li, Y., and Wang, J.: Occurrence, impacts, and microbial transformation of 3-methylindole (skatole): A critical review, J. Hazard. Mater., 416, 126181, https://doi.org/10.1016/j.jhazmat.2021.126181, 2021.

MacLeod, M., Scheringer, M., Podey, H., Jones, K. C., and Hungerbühler, K.: The Origin and Significance of Short-Term Variability of Semivolatile Contaminants in Air, Environ. Sci. Technol., 41, 3249–3253, https://doi.org/10.1021/es062135w, 2007.

McKee, M. L., Nicolaides, A., and Radom, L.: A Theoretical Study of Chlorine Atom and Methyl Radical Addition to Nitrogen Bases: Why Do Cl Atoms Form Two-Center-Three-Electron Bonds Whereas CH_3 Radicals Form Two-Center-Two-Electron Bonds, J. Am. Chem. Soc., 118, 10571–10576, https://doi.org/10.1021/ja9613973, 1996.

Misztal, P. K., Hewitt, C. N., Wildt, J., Blande, J. D., Eller, A. S. D., Fares, S., Gentner, D. R., Gilman, J. B., Graus, M., Greenberg, J., Guenther, A. B., Hansel, A., Harley, P., Huang, M., Jardine, K., Karl, T., Kaser, L., Keutsch, F. N., Kiendler-Scharr, A., Kleist, E., Lerner, B. M., Li, T., Mak, J., Nölscher, A. C., Schnitzhofer, R., Sinha, V., Thornton, B., Warneke, C., Wegener, F., Werner, C., Williams, J., Worton, D. R., Yassaa, N., and Goldstein, A. H.: Atmospheric benzenoid emissions from plants rival those from fossil fuels, Sci. Rep.-UK, 5, 12064, https://doi.org/10.1038/srep12064, 2015.

Montgomery, J. A., Frisch, M. J., Ochterski, J. W., and Petersson, G. A.: A complete basis set model chemistry. VI. Use of density functional geometries and frequencies, J. Chem. Phys., 110, 2822–2827, https://doi.org/10.1063/1.477924, 1999.

Montoya-Aguilera, J., Horne, J. R., Hinks, M. L., Fleming, L. T., Perraud, V., Lin, P., Laskin, A., Laskin, J., Dabdub, D., and Nizkorodov, S. A.: Secondary organic aerosol from atmospheric photooxidation of indole, Atmos. Chem. Phys., 17, 11605–11621, https://doi.org/10.5194/acp-17-11605-2017, 2017.

Nicovich, J. M., Mazumder, S., Laine, P. L., Wine, P. H., Tang, Y., Bunkan, A. J. C., and Nielsen, C. J.: An experimental and theoretical study of the gas phase kinetics of atomic chlorine reactions with CH_3NH_2, $(CH_3)_2NH$, and $(CH_3)_3N$, Phys. Chem. Chem. Phys., 17, 911–917, https://doi.org/10.1039/C4CP03801K, 2015.

Nielsen, C. J., Herrmann, H., and Weller, C.: Atmospheric chemistry and environmental impact of the use of amines in carbon capture and storage (CCS), Chem. Soc. Rev., 41, 6684–6704, https://doi.org/10.1039/C2CS35059A, 2012.

Onel, L., Blitz, M., Dryden, M., Thonger, L., and Seakins, P.: Branching Ratios in Reactions of OH Radicals with Methylamine, Dimethylamine, and Ethylamine, Environ. Sci. Technol., 48, 9935–9942, https://doi.org/10.1021/es502398r, 2014a.

Onel, L., Dryden, M., Blitz, M. A., and Seakins, P. W.: Atmospheric Oxidation of Piperazine by OH has a Low Potential to Form Carcinogenic Compounds, Environ. Sci. Technol. Lett., 1, 367–371, https://doi.org/10.1021/ez5002159, 2014b.

Praske, E., Otkjær, R. V., Crounse, J. D., Hethcox, J. C., Stoltz, B. M., Kjaergaard, H. G., and Wennberg, P. O.: Atmospheric autoxidation is increasingly important in urban and suburban North America, P. Natl. Acad. Sci. USA, 115, 64, https://doi.org/10.1073/pnas.1715540115, 2018.

Reed, A. E., Weinstock, R. B., and Weinhold, F.: Natural population analysis, J. Chem. Phys., 83, 735–746, https://doi.org/10.1063/1.449486, 1985.

Ren, Z. and da Silva, G.: Atmospheric Oxidation of Piperazine Initiated by OH: A Theoretical Kinetics Investigation, ACS Earth Space Chem., 3, 2510–2516, https://doi.org/10.1021/acsearthspacechem.9b00227, 2019.

Riedel, T. P., Bertram, T. H., Crisp, T. A., Williams, E. J., Lerner, B. M., Vlasenko, A., Li, S.-M., Gilman, J., de Gouw, J., Bon, D. M., Wagner, N. L., Brown, S. S., and Thornton, J. A.: Nitryl Chloride and Molecular Chlorine in the Coastal Marine Boundary Layer, Environ. Sci. Technol., 46, 10463–10470, https://doi.org/10.1021/es204632r, 2012.

Rienstra-Kiracofe, J. C., Allen, W. D., and Schaefer, H. F.: The $C_2H_5 + O_2$ Reaction Mechanism: High-Level ab Initio Characterizations, J. Phys. Chem. A, 104, 9823–9840, https://doi.org/10.1021/jp001041k, 2000.

Robinson, P. J. and Holbrook, K. A.: Unimolecular Reactions, John Wiley & Sons: New York, ISBN 0471728144, 1972.

Schade, G. W. and Crutzen, P. J.: Emission of aliphatic amines from animal husbandry and their reactions: Potential source of N_2O and HCN, J. Atmos. Chem., 22, 319–346, https://doi.org/10.1007/BF00696641, 1995.

SenGupta, S., Indulkar, Y., Kumar, A., Dhanya, S., Naik, P. D., and Bajaj, P. N.: Kinetics of Gas-Phase Reaction of OH with Morpholine: An Experimental and Theoretical Study, J. Phys. Chem. A, 114, 7709–7715, https://doi.org/10.1021/jp101464x, 2010.

Shen, J., Xie, H.-B., Elm, J., Ma, F., Chen, J., and Vehkamäki, H.: Methanesulfonic Acid-driven New Particle Formation Enhanced by Monoethanolamine: A Computational Study, Environ. Sci. Technol., 53, 14387–14397, https://doi.org/10.1021/acs.est.9b05306, 2019.

Shen, J., Elm, J., Xie, H.-B., Chen, J., Niu, J., and Vehkamäki, H.: Structural Effects of Amines in Enhancing Methanesulfonic Acid-Driven New Particle Formation, Environ. Sci. Technol., 54, 13498–13508, https://doi.org/10.1021/acs.est.0c05358, 2020.

Shiels, O. J., Kelly, P. D., Bright, C. C., Poad, B. L. J., Blanksby, S. J., da Silva, G., and Trevitt, A. J.: Reactivity Trends in the Gas-Phase Addition of Acetylene to the N-Protonated Aryl Radical Cations of Pyridine, Aniline, and Benzonitrile, J. Am. Soc. Mass. Spectrom., 32, 537–547, https://doi.org/10.1021/jasms.0c00386, 2021.

Silva, P. J., Erupe, M. E., Price, D., Elias, J., G. J. Malloy, Q., Li, Q., Warren, B., and Cocker, D. R.: Trimethylamine as Precursor to Secondary Organic Aerosol Formation via Nitrate Radical Reaction in the Atmosphere, Environ. Sci. Technol., 42, 4689–4696, https://doi.org/10.1021/es703016v, 2008.

Tan, W., Zhu, L., Mikoviny, T., Nielsen, C. J., Wisthaler, A., D'Anna, B., Antonsen, S., Stenstrøm, Y., Farren, N. J., Hamilton, J. F., Boustead, G. A., Brennan, A. D., Ingham, T., and Heard, D. E.: Experimental and Theoretical Study of the OH-Initiated Degradation of Piperazine under Simulated Atmospheric Conditions, J. Phys. Chem. A, 125, 411–422, https://doi.org/10.1021/acs.jpca.0c10223, 2021.

Thornton, J. A., Kercher, J. P., Riedel, T. P., Wagner, N. L., Cozic, J., Holloway, J. S., Dubé, W. P., Wolfe, G. M., Quinn, P. K., Middlebrook, A. M., Alexander, B., and Brown, S. S.: A large atomic chlorine source inferred from mid-continental reactive nitrogen chemistry, Nature, 464, 271–274, https://doi.org/10.1038/nature08905, 2010.

Veres, P. R., Neuman, J. A., Bertram, T. H., Assaf, E., Wolfe, G. M., Williamson, C. J., Weinzierl, B., Tilmes, S., Thompson, C. R., Thames, A. B., Schroder, J. C., Saiz-Lopez, A., Rollins, A. W., Roberts, J. M., Price, D., Peischl, J., Nault, B. A., Møller, K. H., Miller, D. O., Meinardi, S., Li, Q., Lamarque, J.-F., Kupc, A., Kjaergaard, H. G., Kinnison, D., Jimenez, J. L., Jernigan, C. M., Hornbrook, R. S., Hills, A., Dollner, M., Day, D. A., Cuevas, C. A., Campuzano-Jost, P., Burkholder, J., Bui, T. P., Brune, W. H., Brown, S. S., Brock, C. A., Bourgeois, I., Blake, D. R., Apel, E. C., and Ryerson, T. B.: Global airborne sampling reveals a previously unobserved dimethyl sulfide oxidation mechanism in the marine atmosphere, P. Natl. Acad. Sci. USA, 117, 4505, https://doi.org/10.1073/pnas.1919344117, 2020.

Wang, D. S. and Ruiz, L. H.: Secondary organic aerosol from chlorine-initiated oxidation of isoprene, Atmos. Chem. Phys.,

17, 13491–13508, https://doi.org/10.5194/acp-17-13491-2017, 2017.

Wang, K., Wang, W. G., and Fan, C. C.: Reactions of C_{12}-C_{14} N-Alkylcyclohexanes with Cl Atoms: Kinetics and Secondary Organic Aerosol Formation, Environ. Sci. Technol., 56, 4859–4870, https://doi.org/10.1021/acs.est.1c08958, 2022.

Wang, S. and Wang, L.: The atmospheric oxidation of dimethyl, diethyl, and diisopropyl ethers. The role of the intramolecular hydrogen shift in peroxy radicals, Phys. Chem. Chem. Phys., 18, 7707–7714, https://doi.org/10.1039/C5CP07199B, 2016.

Wang, S., Wu, R., Berndt, T., Ehn, M., and Wang, L.: Formation of Highly Oxidized Radicals and Multifunctional Products from the Atmospheric Oxidation of Alkylbenzenes, Environ. Sci. Technol., 51, 8442–8449, https://doi.org/10.1021/acs.est.7b02374, 2017.

Wang, S., Riva, M., Yan, C., Ehn, M., and Wang, L.: Primary Formation of Highly Oxidized Multifunctional Products in the OH-Initiated Oxidation of Isoprene: A Combined Theoretical and Experimental Study, Environ. Sci. Technol., 52, 12255–12264, https://doi.org/10.1021/acs.est.8b02783, 2018.

Wu, R., Wang, S., and Wang, L.: New Mechanism for the Atmospheric Oxidation of Dimethyl Sulfide. The Importance of Intramolecular Hydrogen Shift in a CH_3SCH_2OO Radical, J. Phys. Chem. A, 119, 112–117, https://doi.org/10.1021/jp511616j, 2015.

Xia, M., Peng, X., Wang, W., Yu, C., Sun, P., Li, Y., Liu, Y., Xu, Z., Wang, Z., Xu, Z., Nie, W., Ding, A., and Wang, T.: Significant production of $ClNO_2$ and possible source of Cl_2 from N_2O_5 uptake at a suburban site in eastern China, Atmos. Chem. Phys., 20, 6147–6158, https://doi.org/10.5194/acp-20-6147-2020, 2020.

Xie, H. B., Li, C., He, N., Wang, C., Zhang, S., and Chen, J. W.: Atmospheric Chemical Reactions of Monoethanolamine Initiated by OH Radical: Mechanistic and Kinetic Study, Environ. Sci. Technol., 48, 1700–1706, https://doi.org/10.1021/es405110t, 2014.

Xie, H. B., Ma, F.F., Wang, Y., He, N., Yu, Q., and Chen, J. W.: Quantum Chemical Study on •Cl-Initiated Atmospheric Degradation of Monoethanolamine, Environ. Sci. Technol., 49, 13246–13255, https://doi.org/10.1021/acs.est.5b03324, 2015.

Xie, H. B., Ma, F.F., Yu, Q., He, N., and Chen, J. W.: Computational Study of the Reactions of Chlorine Radicals with Atmospheric Organic Compounds Featuring NH_x-π-Bond ($x = 1$, 2) Structures, J. Phys. Chem. A, 121, 1657–1665, https://doi.org/10.1021/acs.jpca.6b11418, 2017.

Young, C. J., Washenfelder, R. A., Edwards, P. M., Parrish, D. D., Gilman, J. B., Kuster, W. C., Mielke, L. H., Osthoff, H. D., Tsai, C., Pikelnaya, O., Stutz, J., Veres, P. R., Roberts, J. M., Griffith, S., Dusanter, S., Stevens, P. S., Flynn, J., Grossberg, N., Lefer, B., Holloway, J. S., Peischl, J., Ryerson, T. B., Atlas, E. L., Blake, D. R., and Brown, S. S.: Chlorine as a primary radical: evaluation of methods to understand its role in initiation of oxidative cycles, Atmos. Chem. Phys., 14, 3427–3440, https://doi.org/10.5194/acp-14-3427-2014, 2014.

Yu, D., Tan, Z., Lu, K., Ma, X., Li, X., Chen, S., Zhu, B., Lin, L., Li, Y., Qiu, P., Yang, X., Liu, Y., Wang, H., He, L., Huang, X., and Zhang, Y.: An explicit study of local ozone budget and NO_s-VOCs sensitivity in Shenzhen China, Atmos. Environ., 224, 117304, https://doi.org/10.1016/j.atmosenv.2020.117304, 2020.

Yu, F. and Luo, G.: Modeling of gaseous methylamines in the global atmosphere: impacts of oxidation and aerosol uptake, Atmos. Chem. Phys., 14, 12455–12464, https://doi.org/10.5194/acp-14-12455-2014, 2014.

Yu, Q., Xie, H. B., and Chen, J. W.: Atmospheric chemical reactions of alternatives of polybrominated diphenyl ethers initiated by OH: A case study on triphenyl phosphate, Sci. Total Environ., 571, 1105–1114, https://doi.org/10.1016/j.scitotenv.2016.07.105, 2016.

Yu, Q., Xie, H. B., Li, T., Ma, F., Fu, Z., Wang, Z., Li, C., Fu, Z., Xia, D., and Chen, J. W.: Atmospheric chemical reaction mechanism and kinetics of 1,2-bis(2,4,6-tribromophenoxy)ethane initiated by OH radical: a computational study, RSC Adv., 7, 9484–9494, https://doi.org/10.1039/C6RA26700A, 2017.

Yuan, B., Coggon, M. M., Koss, A. R., Warneke, C., Eilerman, S., Peischl, J., Aikin, K. C., Ryerson, T. B., and de Gouw, J. A.: Emissions of volatile organic compounds (VOCs) from concentrated animal feeding operations (CAFOs): chemical compositions and separation of sources, Atmos. Chem. Phys., 17, 4945–4956, https://doi.org/10.5194/acp-17-4945-2017, 2017.

Zhang, R., Wang, G., Guo, S., Zamora, M. L., Ying, Q., Lin, Y., Wang, W., Hu, M., and Wang, Y.: Formation of Urban Fine Particulate Matter, Chem. Rev., 115, 3803–3855, https://doi.org/10.1021/acs.chemrev.5b00067, 2015.

Zhang, Z., Lin, L., and Wang, L.: Atmospheric oxidation mechanism of naphthalene initiated by OH radical. A theoretical study, Phys. Chem. Chem. Phys., 14, 2645–2650, https://doi.org/10.1039/C2CP23271E, 2012.

Zhao, Y. and Truhlar, D. G.: The M06 suite of density functionals for main group thermochemistry, thermochemical kinetics, noncovalent interactions, excited states, and transition elements: two new functionals and systematic testing of four M06-class functionals and 12 other functionals, Theor. Chem. Acc., 120, 215–241, https://doi.org/10.1007/s00214-007-0310-x, 2008.

Zito, P., Dötterl, S., and Sajeva, M.: Floral Volatiles in a Sapromyiophilous Plant and Their Importance in Attracting House Fly Pollinators, J. Chem. Ecolo., 41, 340–349, https://doi.org/10.1007/s10886-015-0568-8, 2015.